

## SWIFT-BAT HARD X-RAY SKY MONITORING UNVEILS THE ORBITAL PERIOD OF THE HMXB IGR J18219–1347

V. LA PAROLA<sup>1</sup>, G. CUSUMANO<sup>1</sup>, A. SEGRETO<sup>1</sup>, A. D’AÌ<sup>2</sup>, N. MASETTI<sup>3</sup>, V. D’ELIA<sup>4,5</sup>

*Draft version October 8, 2018*

### ABSTRACT

IGR J18219–1347 is a hard X-ray source discovered by INTEGRAL in 2010. We have analyzed the X-ray emission of this source exploiting the BAT survey data up to March 2012 and the XRT data that include also an observing campaign performed in early 2012. The source is detected at a significance level of  $\sim 13$  standard deviations in the 88-month BAT survey data, and shows a strong variability along the survey monitoring, going from high intensity to quiescent states. A timing analysis on the BAT data revealed an intensity modulation with a period of  $P_0 = 72.44 \pm 0.3$  days. The significance of this modulation is about 7 standard deviations in Gaussian statistics. We interpret it as the orbital period of the binary system. The light curve folded at  $P_0$  shows a sharp peak covering  $\sim 30\%$  of the period, superimposed to a flat level roughly consistent with zero. In the soft X-rays the source is detected only in 5 out of 12 XRT observations, with the highest recorded count rate corresponding to a phase close to the BAT folded light curve peak. The long orbital period and the evidence that the source emits only during a small fraction of the orbit suggests that the IGR J18219–1347 binary system hosts a Be star. The broad band XRT+BAT spectrum is well modeled with a flat absorbed power law with a high energy exponential cutoff at  $\sim 11$  keV.

*Subject headings:* X-rays: binaries — X-rays: individual (IGR J18219–1347)

### 1. INTRODUCTION

The INTEGRAL observatory (Winkler et al. 2003) with the IBIS/ISGRI telescope (Ubertini et al. 2003; Lebrun et al. 2003) and the Swift observatory (Gehrels et al. 2004) with the Burst Alert Telescope (BAT, Barthelmy 2005) are performing a continuous monitoring of the sky in the hard X-ray energy band offering a long-term database for the activity of the X-ray sources and a large number of new detections of transient or very faint accreting sources. Most of the recently discovered high-mass X-ray binaries (HMXBs) are characterized by high local absorption ( $N_{\text{H}} > 10^{22} \text{ cm}^{-2}$ ) that prevented their detection by past soft X-ray monitoring. The BAT telescope is complementary to IBIS/ISGRI for the study of the temporal behavior of these sources as it covers a fraction between 50% and 80% of the sky every day thanks to its large field of view (1.4 steradian half coded) and to its pointing strategy. The long (since 2004 December 15) and continuous monitoring has allowed to investigate the intrinsic emission variability and to search for the presence of long periodicities, unveiling the binary nature of many INTEGRAL sources (e.g. Corbet & Krimm 2009; Corbet et al. 2010a,b,c,d,e; Corbet & Krimm 2010; Cusumano et al. 2010; La Parola et al. 2010; D’Aì et al. 2011).

In this Letter we analyze the soft and hard X-ray data collected by Swift on IGR J18219–1347. The source was discovered by INTEGRAL (Krivonos et al. 2010) and it was associated with XMMSL1 J182155.0–134719 because of a spatial coincidence. A 2MASS object (2MASS 18215463–1347232)

found within the XMM counterpart position error box was initially identified as the infrared counterpart of the IGR source (Landi et al. 2011). IGR J18219–1347 was also detected by BAT (Krimm et al. 2012) at the end of January 2012, with an intensity rising of a factor of 10 in 7 days: the average 17–60 keV flux was  $2 \times 10^{-10} \text{ erg cm}^{-2} \text{ s}^{-1}$ , more than 25 times the flux measured by INTEGRAL (Krivonos et al. 2010). The BAT detection triggered a Swift-XRT (Burrows et al. 2005) follow up observing campaign allowing to obtain a refined position with a localization accuracy of  $1.7''$ , confirming the soft X-ray counterpart XMMSL1 J182155.0–134719 and rejecting the infrared counterpart candidate 2MASS 18215463–1347232 (Krimm et al. 2012). The *Swift*-XRT observations also revealed strong evidence for variability with an intensity variation at least of a factor of 50. A follow-up observation with Chandra found a soft X-ray counterpart at a position of  $\text{RA}_{J2000} = 18\text{h } 21\text{m } 54.82\text{s}$ ,  $\text{Dec}_{J2000} = -13^\circ 47' 26.7''$  with a localization accuracy of  $0.64''$ , thus reducing the area of position uncertainty of a factor of 6 (Karasev et al. 2012). The Chandra source position was cross correlated with the UKIDSS<sup>6</sup> sky survey data allowing to identify an infrared source at  $\text{RA}_{J2000} = 18\text{h } 21\text{m } 54.766\text{s}$ ,  $\text{Dec}_{J2000} = -13^\circ 47' 26.77''$ , at a distance of  $\sim 0.8''$ , with magnitudes  $J=18.00$ ,  $H=16.01$ , and  $K=14.44$ , as the likely counterpart. An accurate study of the profile of the image of this source showed, however, that it is likely the superposition of two sources that cannot be separated because of the spatial resolution of the infrared data.

Broad band (0.5–100 keV) spectral analysis combining *Swift*-XRT and INTEGRAL/IBIS data was modeled with an absorbed power law ( $N_{\text{H}} \sim 3 \times 10^{22} \text{ cm}^{-2}$ , photon index  $\sim 1$  and an exponential cutoff at  $\sim 6$  keV; Karasev et al. (2012)). The information derived from the broad band spectrum analysis and the strong variability suggested that IGR J18219–1347 belongs to the class of the HMXBs.

This Letter is organized as follows. Section 2 describes the

laparola@ifc.inaf.it

<sup>1</sup> INAF, Istituto di Astrofisica Spaziale e Fisica Cosmica, Via U. La Malfa 153, I-90146 Palermo, Italy

<sup>2</sup> Dipartimento di Fisica e Chimica, Università di Palermo, via Archirafi 36, 90123, Palermo, Italy

<sup>3</sup> INAF - Istituto di Astrofisica Spaziale e Fisica Cosmica di Bologna, via Gobetti 101, 40129, Bologna, Italy

<sup>4</sup> INAF - Osservatorio Astronomico di Roma, Via Frascati 33, I-00040 Monteporzio Catone, Italy

<sup>5</sup> ASI-Science Data Centre, Via Galileo Galilei, I-00044 Frascati, Italy

<sup>6</sup> <http://www.ukidss.org/index.html>

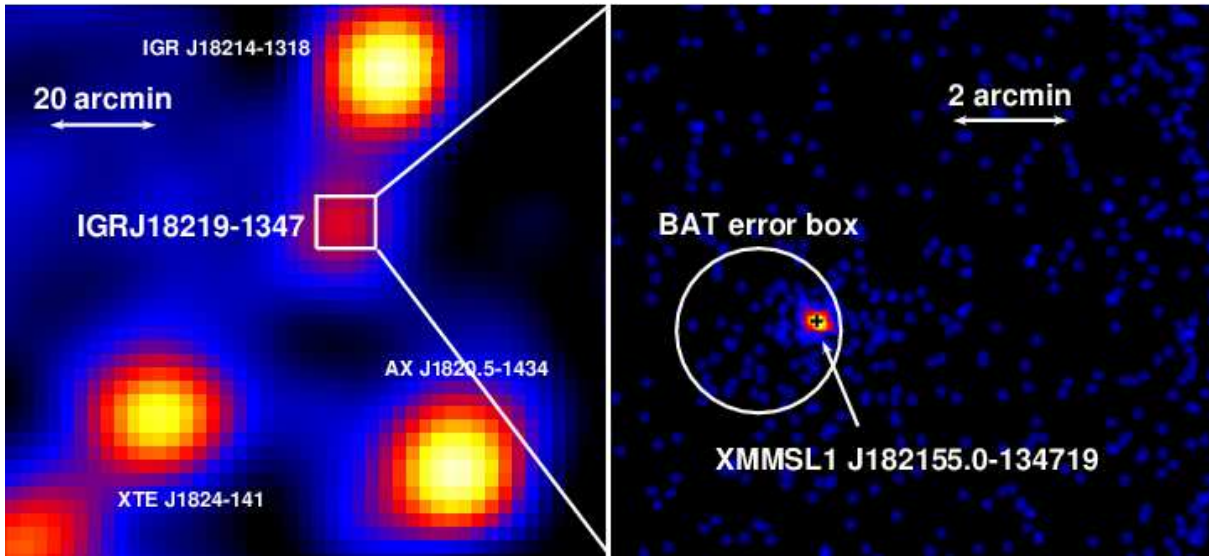


**Figure 1.** Left panel: 15–45 keV significance map in the region around IGR J18219–1347. Right panel: 0.2–10 keV XRT image of observation 1 (see table 1).

data reduction. Section 3 reports on the timing analysis. In Section 4 we describe the spectral analysis and in Section 5 we briefly discuss our results.

## 2. DATA REDUCTION

The BAT survey data (15–150 keV) of the first 88 months of the *Swift* mission (2004 December – 2012 March) were retrieved from the HEASARC public archive<sup>7</sup> and processed with a software (Segreto et al. 2010) dedicated to the analysis of data of coded mask telescopes. The code performs screening, mosaicking and source detection and produces scientific products of any detected source. IGR J18219–1347 was detected in the 15–150 keV at a significance of 12.0 standard deviations, with a maximum of significance (12.7 standard deviations) in the 15–45 keV energy band. Figure 1 (left) shows the 15–45 keV significance sky map (exposure time of 28.1 Ms) centered in the direction of IGR J18219–1347. We extracted the background subtracted spectrum of the source averaged over the entire survey and the light curve in the 15–45 keV energy range with the maximum available time resolution ( $\sim 300$  s). The time tag of each bin of the light curve was corrected to the Solar system barycentre (SSB) using the JPL DE-200 ephemeris (Standish 1982) and the task EARTH2SUN<sup>8</sup>.

*Swift*-XRT observed the field of IGR J18219–1347 on 2010 March 5 in Photon Counting (PC) mode without detecting any source (Obs # 0 in table 1). Two years later (2012 February 15), following the detection of the source as a transient by BAT, a one month target of opportunity campaign was activated. The source was observed in PC mode in the first observation (obs # 1 in table 1) and in Windowed Timing (WT) mode (Hill et al. 2004) in the following observations (obs # 2 to 11 in table 1). The XRT data were processed with standard procedures (XRTPIPELINE v.0.12.4), filtering and screening criteria, using ftools in the Heasoft package (v 6.8). We adopted standard grade filtering 0-12 and 0-2 for PC and WT data, respectively. IGR J18219–1347 was detected only in 5 out of 11 observations. Table 1 reports the details

on the *Swift*-XRT observations and the relevant count rate. Figure 1 (right) shows the 0.2–10 keV XRT image from ObsID 00032285001 where a source consistent in position to the likely soft X-ray counterpart XMMSL1 J182155.0–134719 is detected with a significance of  $\sim 14$  standard deviations. No other sources are detected inside the BAT error box.

The source events for data collected in PC mode (Obs # 1) were extracted from a circular region of 20 pixel radius (1 pixel = 2.36'') centered on the source position as determined with XRTCENTROID while, for data collected in WT mode, events were extracted only from obs. 2, 3, 5 and 6 (see Table 1) by selecting a 20 pixel wide portion of the WT strip centered on the source position. The background for spectral analysis was extracted from an annular region centered on the source with radii of 70 and 130 pixels for the observation in PC mode and from two strip regions (symmetrical with respect to the source position) sufficiently offset ( $> 2$  arcminutes) from the source to avoid any contamination from its PSF wings in WT mode. We used the official BAT spectral redistribution matrix<sup>9</sup> and the XRT spectral redistribution matrix v013. XRT ancillary response files were generated with XRTMKARF<sup>10</sup> Spectral fits were performed using XSPEC v.12. The source and background spectra of the observations in WT mode were combined to obtain a single spectrum, and the ancillary files were combined using ADDARF weighting them by the exposure times of the relevant spectra. Finally, spectra were rebinned with a minimum of 20 counts per energy channel, in order to allow the use of the  $\chi^2$  statistics.

## 3. TIMING ANALYSIS

We analyzed the long term BAT light curve to search for periodic intensity modulation using the epoch folding method (Leahy et al. 1983). The 15–45 keV BAT light curve was folded with different trial periods  $P$  from 0.5 d to 500 d with a step of  $P^2/(N \Delta T)$ , where  $N = 16$  is the number of trial profile phase bins and  $\Delta T = 211.7$  Ms is the data time span. To build profiles for each trial period we applied a weighing procedure (e.g. Cusumano et al. 2010) suitable for background

<sup>7</sup> <http://heasarc.gsfc.nasa.gov/docs/archive.html>

<sup>8</sup> <http://heasarc.gsfc.nasa.gov/ftools/fhelp/earth2sun.txt>

<sup>9</sup> <http://heasarc.gsfc.nasa.gov/docs/heasarc/caldb/data/swift/bat/index.html>

<sup>10</sup> <http://heasarc.gsfc.nasa.gov/ftools/caldb/help/xrtmkarf.html>

Obs #	Instrument mode	Obs ID	$T_{start}$ (TDB) (MJD)	$T_{elapsed}$ (s)	Exposure (s)	Rate (c/s)	Orb. Phase
0	XRT-PC	00031649001	55260.7956	17647.1	1253.7	<0.002	0.86
1	XRT-PC	00032285001	55972.2877	39461.7	1183.7	$0.17 \pm 0.01$	0.68
2	XRT-WT	00032285002	55978.6860	24777.1	1786.2	$0.056 \pm 0.012$	0.77
3	XRT-WT	00032285003	55981.7045	12850.7	2691.8	$0.0682 \pm 0.009$	0.81
4	XRT-WT	00032285004	55984.1737	24217.0	2935.5	<0.025	0.84
5	XRT-WT	00032285005	55987.6437	13019.6	1476.7	$0.027 \pm 0.009$	0.89
6	XRT-WT	00032285006	55990.5850	24750.7	1247.3	$0.022 \pm 0.011$	0.93
7	XRT-WT	00032285007	55993.0593	7396.7	2797.1	<0.022	0.96
8	XRT-WT	00032285008	55996.0047	5457.5	1462.8	<0.027	0.01
9	XRT-WT	00032285009	55999.0754	24613.9	2604.3	<0.021	0.05
10	XRT-WT	00032285010	56003.765	18656.8	3048.0	<0.021	0.11
11	XRT-WT	00032285011	56005.7693	7452.3	2814.0	<0.024	0.14

**Table 1**  
Log of the Swift-XRT observations.

dominated data with a large span of count rate errors. Figure 2a shows the periodogram, where several features emerge. The highest one has a  $\chi^2$  value of  $\sim 358$  and corresponds to a period of  $P_0 = 72.44 \pm 0.3$  d. From fitting the peak profile with a Gaussian function, we derived a  $P_0$  centroid and a standard deviation of 72.44 d and 0.3 d, respectively. We see also other evident features at periods multiples of  $P_0$  ( $P_1, P_2, P_3, P_4, P_5$  in Fig 2a) and at the sub-multiple  $P_0/2$ . The intensity profile (Fig 2b) folded at  $P_0$  with  $T_{epoch}=54619.3125$  shows a peak that covers 30% of the period, over a flat level consistent with zero. To evaluate the phase position of the peak centroid we have built a pulse profile folding BAT data with  $P_0$ ,  $N = 30$  phase bins and fit the peak with a Gaussian model: the centroid is at phase  $0.510 \pm 0.004$  corresponding to MJD  $(54656.26 \pm 0.29) \pm nP_0$ . The presence of the feature at  $P_0/2$  is a direct consequence of the sharp and narrow peak shown in Figure 2b: folding with a period equal to  $P_0/2$  this peak will be added coherently to the profile every two cycles, producing a feature in the periodogram with an intensity significantly lower with respect to the main feature.

As a consequence of the source variability and of the presence of a periodic signal, the average  $\chi^2$  in the periodogram is far from the average value expected for white noise ( $N - 1$ ) and the  $\chi^2$  statistics cannot be applied. The significance of the observed feature shall be evaluated with respect to the average level of the periodogram noise. For this reason, we fitted the periodogram with a second order polynomial and subtracted the best fit ( $F_\chi$ ) to the  $\chi^2$  distribution. The  $z = \chi^2 - F_\chi$  distribution has a value of  $\sim 304$  at  $P_0$ . We therefore have built the histogram of the  $z$  distribution (Figure 2c) extracting the values only from 22 to 122 d (where the noise level is quite consistent with the noise level at  $P_0$ ) and excluding the interval around  $P_0$  and around  $P_0/2$ . We fit the tail ( $z > 10$ ) of this distribution with an exponential function. The resulting best fit model is plotted in Figure 2c. We have evaluated the area under the histogram dividing it into two parts: from its left boundary up to  $z = 10$  we have summed the contribution of each single bin; beyond  $z = 10$  up to infinity we have integrated the best fit exponential model. Therefore, we evaluated the integral of the best-fit exponential function beyond 304 and normalized it to the total area of the histogram. The result ( $6.7 \times 10^{-12}$ ) is the probability of chance occurrence of a  $z$  equal to or larger than 304 or a  $\chi^2$  equal to or larger than 358 and it corresponds to a significance for the detected feature of  $\sim 7$  standard deviations in Gaussian statistics.

Figure 2d shows the 15–45 keV light curve of IGR J18219–1347 with a bin time of  $P_0/5$ . To visually show the periodicity in the BAT light curve, we over-plotted vertical shaded bars

spaced by  $P_0$  and in phase with the peak of the BAT folded profile (Fig. 2b). Table 1 reports the phase corresponding to each XRT observation relevant to the BAT light curve profile in Figure 2b. We observe that the pointing with the highest count rate corresponds to the phase closest to the peak, while upper limits correspond to orbital phases farther from the peak. The statistics of the source in the XRT dataset both in PC and in WT mode is too low to allow for timing analysis finalized to the search for a pulsation.

#### 4. BROAD BAND SPECTRAL ANALYSIS

Broad band spectral analysis was performed using the XRT data relevant to the observations with the source detected above 2 standard deviations (Obs. 1 in PC mode and Obs. 2, 3, 5 and 6 in WT mode that were summed into a single spectrum because the statistics of each single WT dataset is too low to build a significant spectrum; see table 1 and Sect. 2) and the BAT hard X-ray spectrum averaged over the 88 months of monitoring, selecting only intervals corresponding to the phase of the peak. We assumed no significant spectral variability among the XRT observations and during the BAT monitoring. A preliminary analysis was made to verify that this assumption was indeed valid. The XRT spectra in PC mode and WT mode were fitted simultaneously with an absorbed power-law with the absorption hydrogen column and the photon index parameters forced to have the same value in both datasets. The best fit residuals showed the same trend for both datasets, with a best fit photon index equal to  $-0.2^{+0.9}_{-0.4}$  and absorbing column density equal to  $3.3^{+3}_{-2} \times 10^{22} \text{ cm}^{-2}$ . Six BAT spectra were produced to verify the assumption of non-variability both during the 88-month monitoring (dividing it into four 22-month long intervals) and/or during different phase intervals of Figure 2b (selecting the two spectra corresponding to phase intervals 0.4375–0.625 and 0.625–1.375). These spectra were fitted with a power law model and, as above, the photon index was constrained to have the same value for all the spectra without any constraint for the normalization parameters. The best fit residuals show the same trend for all the datasets, with best fit photon index  $2.64 \pm 0.14$ .

Therefore, assuming no significant spectral variability during the BAT monitoring and between the XRT spectra we performed a broad band spectral analysis coupling the soft X-ray spectra with the BAT spectrum selected in phase with the peak in the folded profile (phase intervals 0.4375 to 0.625 in Figure 2b) introducing in the model a multiplicative factor to take into account both an intercalibration factor between the two telescopes and the different average flux level among the three datasets. An absorbed power law model gave an

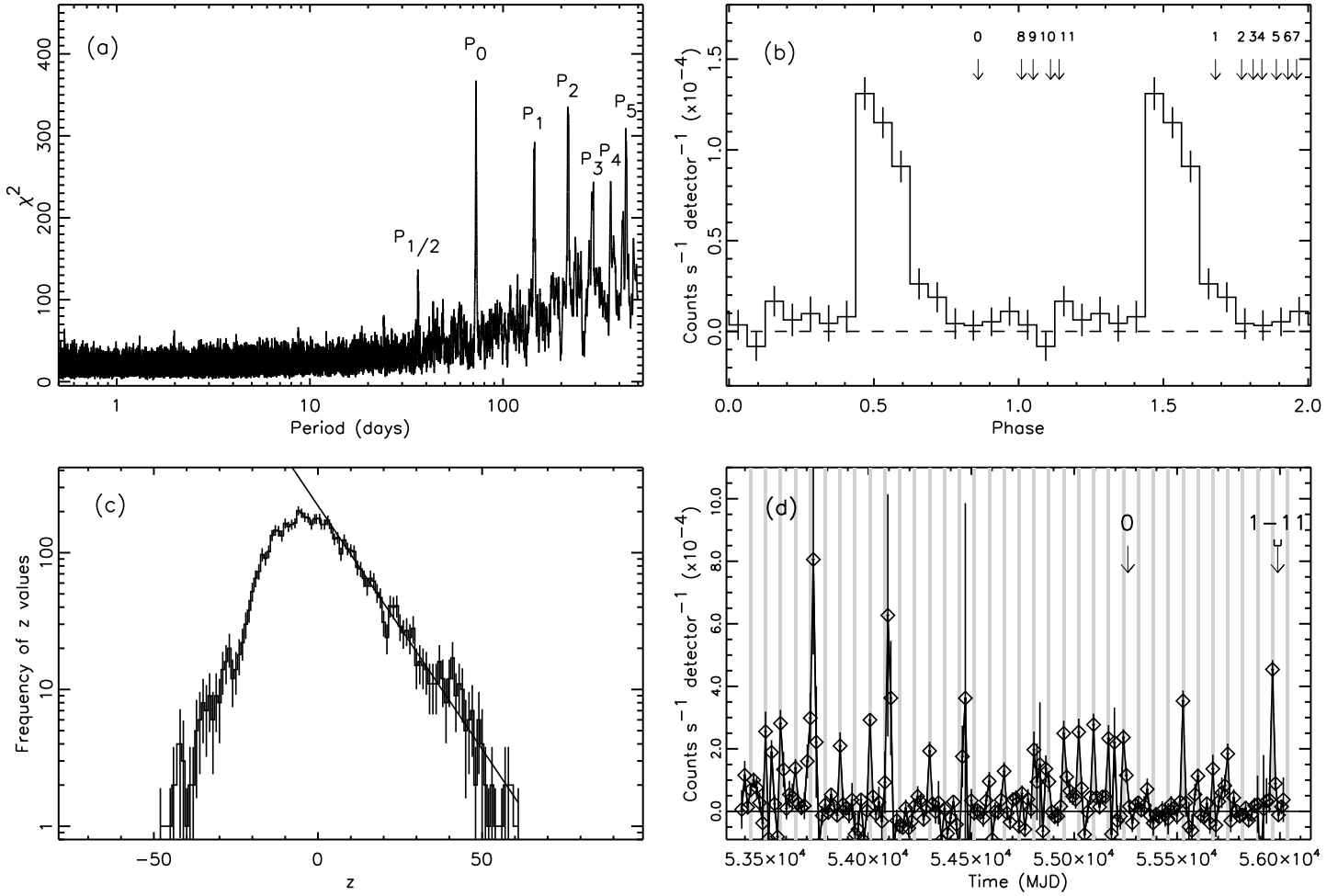


**Figure 2.** **a:** Periodogram of *Swift*/BAT (15–45 keV) data for IGR J18219-1347. **b:** Light curve folded at a period  $P = 72.44$  days, with 16 phase bins. Vertical arrows show the phase position corresponding to the epoch of each XRT observation. **c:** Distribution of  $z$  ( $\chi^2 - F_\chi$ ) selecting  $\chi^2$  between 22 and 122 days and excluding the values around the peak  $P_0$ . The continuous line is the best fit obtained with an exponential model applied to the tail of the distribution (above  $z=22$ ). **d:** 15–45 keV BAT light curve of IGR J18219-1347 with a bin time of  $P_0/5 = 14.49$  d. Vertical arrows show the epoch of the XRT observations (observations from Obs. 1 to 11 were performed within a time interval 33 days long). The shaded lines are spaced by  $P_0 = 72.44$  d and in phase with the peak position in Figure 2b.

unacceptable  $\chi^2$  of 89.21 (52 d.o.f.). This was expected because of the difference in photon index found in the analysis performed separately for the XRT and BAT datasets. The broad-band spectrum resulted indeed well fitted ( $\chi^2=61.7$  (51 d.o.f.) adding to the power law a high energy exponential cut-off (`phabs*cutoffpl` model). Figure 3 shows the combined XRT and BAT energy distribution with best fit model (top panel) and residuals in units of standard deviations (bottom panel). Table 2 reports the best fit parameters (quoted errors are given at 90% confidence level).

## 5. DISCUSSION AND CONCLUSIONS

We have presented the results obtained from the analysis of the data collected by *Swift* on IGR J18219-1347. The first 88 months of BAT survey data show a strong emission variability in the hard X-ray energies with the source going from quiescent to high emission states. The timing analysis performed on the BAT data unveils a periodic modulation of  $P_0=72.44$  days that we interpret as the orbital period of binary system. The profile obtained folding the BAT light curve at  $P_0$  shows a flat plateau consistent with the source being in a quiescent state, and a narrow peak lasting only 30% of the orbital period. The brightness enhancement on 2012 Feb. 6 (MJD 55963), observed by BAT and reported by Krimm et al. (2012), correspond to phase 0.54, fully consistent with the phase of the peak in the folded light curve. The one-month XRT observing campaign that followed this detection shows that the soft X-ray emission is in agreement with the hard X-ray modulation, with the source **strongly** detected only in the observations close to the BAT folded light curve peak (**obs 1 to 3**) and with no or marginal detections (Obs 5 and 6) in the observations corresponding to the plateau. **The non-detection in Obs 4 is** due to a higher background level (a factor of 2 higher than in Obs 5 and 6).

The long orbital period and the evidence that the source emits only during a small fraction of the orbit suggests that the high mass companion of IGR J18219-1347 is a Be star. Be/X-ray binaries are indeed the most numerous class of HMXB and are characterized by wide orbits with moderate eccentricities, as opposite to supergiant X-ray binaries that show circular orbits with periodicities shorter than  $\sim 10$  days (e.g. Liu, van Paradijs & van den Heuvel 2006). In a Be/X-ray binary system the accretion onto the neutron star is driven by mass capture from an equatorial disk around the equatorial plane of the Be star (Okazaki & Negueruela 2001). This is favored at the periastron passage and causes the so-called type-I outbursts, while for most of the orbit a large orbital distance prevents the accretion, keeping the source in a quiescent state. This is consistent with the overall behaviour observed in the BAT light curve of IGR J18219-1347 (Fig. 2d), with the source emission characterized by periodic emission peaks. As observed for Be/X-ray binary systems (Reig & Roche 1999; Reig 2011), the intensity of these peaks show a large variability and is related to the amount of disk material captured for accretion during the periastron passage. Corbet (1986) showed that in Be/X-ray binaries the orbital period tends to be correlated with the spin period. If IGR J18219-1347 is indeed a member of this class, we can expect a spin period longer than 10 s.

The broad-band (0.2–150 keV) spectrum of IGR J18219–1347 is well modeled with a flat absorbed power law with a high energy exponential cutoff at  $\sim 11$  keV. The column density is  $\sim 4.3 \times 10^{22} \text{ cm}^{-2}$ , which is a factor of  $\sim 3$  larger than the Galactic value in the direction of the source

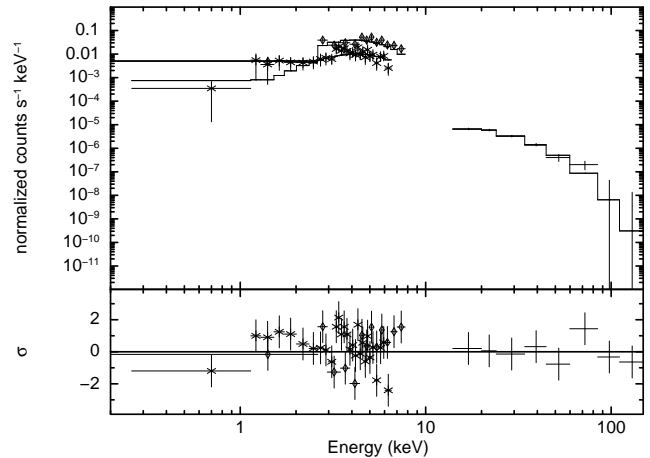


**Figure 3.** Top panel: IGR J18219-1347 XRT (PC: diamond points; WT: star points) and BAT spectra and best fit model. Bottom panel: Residuals in unit of standard deviations.

**Table 2**  
Best fit spectral parameters.

Parameter	Best fit value	Units
$N_{\text{H}}$	$4.3^{+3.8}_{-1.7} \times 10^{22}$	$\text{cm}^{-2}$
$\Gamma$	$-0.1^{+1.1}_{-0.6}$	
$E_{\text{cut}}$	$11^{+8}_{-2}$	keV
$N$	$(7^{+9}_{-5}) \times 10^{-4}$	$\text{ph keV}^{-1} \text{cm}^{-2} \text{s}^{-1}$ at 1 keV
$C_{\text{XRT-WT}}$	$0.26 \pm 0.05$	
$C_{\text{BAT}}$	$0.33^{+0.48}_{-0.14}$	
F (0.2–10 keV)	$4.25 \times 10^{-11}$	$\text{erg s}^{-1} \text{cm}^{-2}$
F (15–150 keV)	$4.23 \times 10^{-11}$	$\text{erg s}^{-1} \text{cm}^{-2}$
$\chi^2$	61.7 (51 d.o.f.)	

**Note.** —  $C_{\text{XRT-WT}}$  and  $C_{\text{BAT}}$  are the constant factors to be multiplied to the model in order to match the XRT-WT and BAT data, respectively. We report unabsorbed fluxes for the standard XRT (0.2–10 keV) and BAT (15–150 keV) energy bands.

( $1.3 \times 10^{22} \text{ cm}^{-2}$  Dickey & Lockman 1990). This suggests an additional intrinsic absorption in the environment of the binary system. These spectral results are in agreement with those reported by Karasev et al. (2012) from the analysis of the XRT/*Swift* and IBIS/INTEGRAL data.

This work was supported in Italy by ASI grant I/011/07/0.

## REFERENCES

- Barthelmy S. D., Barbier L. M., Cummings J. R., et al., 2005, *Space Science Reviews*, 120, 143
- Burrows D. N., Hill J. E., Nousek J. A., et al., 2005, *Space Science Reviews*, 120, 165
- Corbet R. H. D., 1986, *MNRAS*, 220, 1047
- Corbet, R. H. D., & Krimm, H. A. 2009, *The Astronomer’s Telegram*, 2008, 1
- Corbet, R. H. D., Krimm, H. A., & Skinner, G. K. 2010, *The Astronomer’s Telegram*, 2559, 1
- Corbet, R. H. D., Krimm, H. A., Barthelmy, S. D., et al. 2010, *The Astronomer’s Telegram*, 2570, 1
- Corbet, R. H. D., Barthelmy, S. D., Baumgartner, W. H., et al. 2010, *The Astronomer’s Telegram*, 2588, 1
- Corbet, R. H. D., Barthelmy, S. D., Baumgartner, W. H., et al. 2010, *The Astronomer’s Telegram*, 2598, 1
- Corbet, R. H. D., Barthelmy, S. D., Baumgartner, W. H., et al. 2010, *The Astronomer’s Telegram*, 2599, 1
- Corbet, R. H. D., & Krimm, H. A. 2010, *The Astronomer’s Telegram*, 3079, 1

- Cusumano, G., La Parola, V., Romano, P., et al. 2010, MNRAS, 406, L16  
D'Ai, A., La Parola, V., Cusumano, G., et al. 2011, A&A, 529, A30  
Dickey, J. M., & Lockman, F. J. 1990, ARA&A, 28, 215  
Gehrels N., Chincarini G., Giommi P., et al., 2004, ApJ, 611, 1005  
Hill J. E., Burrows, D. N., Nousek J. A. et al., 2004, SPIE, 5165, 217  
Landi, R., Bassani, L., Masetti, N., Bazzano, A., & Bird, A. J. 2011, The Astronomer's Telegram, 3272, 1  
Leahy, D. A., Darbro, W., Elsner, R. F., et al. 1983, ApJ, 266, 160  
Liu Q. Z., van Paradijs J., van den Heuvel E. P. J., 2006, A&A, 455, 1165  
Karasev, D. I., Lutovinov, A. A., Revnivtsev, M. G., & Krivonos, R. A. 2012, Astronomy Letters, 38, 629  
Krimm, H. A., Kennea, J. A., Holland, S. T., et al. 2012, The Astronomer's Telegram, 3933, 1  
Krivonos R., Tsygankov S., Revnivtsev, M., Grebenev, S., Churazov, E., Sunyaev, R., 2010, A&A, 523, 61  
La Parola, V., Cusumano, G., Romano, P., et al. 2010, MNRAS, 405, L66  
Lebrun F., Leray, J. P., Lavocat, P., et al., 2003, A&A, 411, L141  
Okazaki A. T., Negueruela I., 2001, A&A, 377, 161  
Reig, P. 2011, Ap&SS, 332, 1  
Reig, P., & Roche, P. 1999, MNRAS, 306, 100  
Segreto, A., Cusumano, G., Ferrigno, C., La Parola, V., Mangano, V., Mineo, T., & Romano, P. 2010, A&A, 510, A47  
Standish, E. M., Jr. 1982, A&A, 114, 297  
Ubertini P., Lebrun, F., Di Cocco, G., et al., 2003, A&A, 411, L131  
Winkler C., Courvoisier, T. J.-L., Di Cocco, G., et al., 2003, A&A, 411, L1